LETTER Communicated by Laurence Abbott

An Algorithm for Modifying Neurotransmitter Release Probability Based on Pre- and Postsynaptic Spike Timing

Walter Senn
Department of Neurobiology, Weizmann Institute, Rehovot 76100, Israel, and Physiologisches Institut, Universität Bern, Bühlplatz 5, CH-3012 Bern, Switzerland

Henry Markram
Misha Tsodyks
Department of Neurobiology, Weizmann Institute, Rehovot 76100, Israel

The precise times of occurrence of individual pre- and postsynaptic action potentials are known to play a key role in the modification of synaptic efficacy. Based on stimulation protocols of two synaptically connected neurons, we infer an algorithm that reproduces the experimental data by modifying the probability of vesicle discharge as a function of the relative timing of spikes in the pre- and postsynaptic neurons. The primary feature of this algorithm is an asymmetry with respect to the direction of synaptic modification depending on whether the presynaptic spikes precede or follow the postsynaptic spike. Specifically, if the presynaptic spike occurs up to 50 ms before the postsynaptic spike, the probability of vesicle discharge is upregulated, while the probability of vesicle discharge is downregulated if the presynaptic spike occurs up to 50 ms after the postsynaptic spike. When neurons fire irregularly with Poisson spike trains at constant mean firing rates, the probability of vesicle discharge converges toward a characteristic value determined by the pre- and postsynaptic firing rates. On the other hand, if the mean rates of the Poisson spike trains slowly change with time, our algorithm predicts modifications in the probability of release that generalize Hebbian and Bienenstock-Cooper-Munro rules. We conclude that the proposed spike-based synaptic learning algorithm provides a general framework for regulating neurotransmitter release probability.

1 Introduction

Since the work of D. Hebb (1949), several attempts were made to formulate precise learning rules that could enable one to determine the change in synaptic efficacies from the known activities of neurons (Sejnowski, 1977; Bienenstock, Cooper, & Munro, 1982; Artola & Singer, 1993; Fregnac & Shulz, 1994). In these rules neuronal activities are represented by an analog vari-

able reflecting the average firing rates of the neurons. Such formulations were used in training neural networks to perform various computational tasks.

Recent experiments indicate that the relative timing of pre- and postsynaptic activity is crucial in determining the magnitude and direction of synaptic modifications (Gustafsson, Wigström, Abraham, & Huang, 1987; Fregnac, Shulz, Thorpe, & Bienenstock, 1988; Stanton & Sejnowski, 1989; Tsumoto, 1990; Debanne, Shulz, & Fregnac, 1995; Bell, Han, Sugawara, & Grant, 1997; Zhang, Tao, Holt, Harris, & Poo, 1998; Bi & Poo, 1998). In particular, Markram, Lübke, Frotscher, & Sakmann (1997) reported that synaptic modification depends on the millisecond relative timing between the pre- and postsynaptic spikes. They found that if presynaptic spikes occur 10 ± 2 ms before the postsynaptic one, then synaptic responses were increased, while the same pattern of stimulation with the opposite time delay resulted in a decrease of responses. In addition, Markram and Tsodyks (1996) showed that the synaptic modification at this synaptic connection is not a uniform scaling of synaptic strength, but rather a redistribution of synaptic efficacy between the spikes in the train. This redistribution can result from the increase in the probability of neurotransmitter release (Tsodyks & Markram, 1997).

The experiments of Markram et al. (1997) provide for the first time the experimental basis for formulating the synaptic learning rules based on individual spikes rather than firing rates. In this article, we present a phenomenological model that reproduces the experimental results and allows the computation of the synaptic modification for arbitrary patterns of spikes. This model can now be tested against other experimental paradigms and provides a useful foundation for computational models that utilize exact spike timing for information processing (see, e.g., Hopfield, 1995). We think that the restriction to the relative spike timing in describing synaptic long-term modifications is a useful simplification that reduces the wealth of possible molecular mechanisms to the functionally relevant behavior of the neurons.

We also investigate the mean-field behavior of our model when applying Poisson spike trains and compare this with existing learning rules based on firing rates. We found that as a function of the postsynaptic activity, our rule has an anti-Hebbian and a Hebbian regime similar to the Bienenstock-Cooper-Munro (BCM) rule. It also reproduces a sliding threshold property similar to the BCM theory. Moreover, by setting the synaptic parameters, it is possible to generate different types of Hebbian modifications that are closer to a covariance, a Hebbian, or an anti-Hebbian rule. We consider simplifications of our physiologically motivated algorithm and provide a minimal model for an asymmetric spike-based learning rule for the vesicle release probability. Finally, the nonlinearities in our model are put into relation to other spike-based learning rules focusing on aspects of synaptic stability and sensitivity (Abbott & Song, 1999; Kempter, Gerstner, & van Hemmen,

1999a, 1999b). A short form of this work is published in Senn, Tsodyks, and Markram (1997).

2 The Model

Our scheme enables the adaptation of the probability of neurotransmitter release resulting from simultaneous activity of pre- and postsynaptic neurons. Specifically, we adapt the probability that a presynaptic spike discharges a vesicle that is ready at the site of release. We refer to this probability as the probability of discharge, P_{dis}. The biophysical processes involved in modifying P_{dis} are triggered by either a postsynaptic spike or a presynaptic release. Upregulation of P_{dis} is assumed to be induced by a postsynaptic spike following a presynaptic release. Downregulation of P_{dis}, on the other hand, is induced by a presynaptic release following a postsynaptic spike.

Practically, long-lasting synaptic modification does not instantaneously follow the pairing but develops slowly, peaking 10 to 20 minutes after the pairing. Accordingly, while implementing the algorithm, P_{dis} is kept fixed and effects of each spike are summed up to determine the overall change in the limit probability, denoted as P^{∞}_{dis}. This work does not include a short-lasting upregulation of P_{dis} analogous to post-tetanic potentiation because this phenomenon is not clearly evident at these depressing synapses. Also not considered is any decay of P^{∞}_{dis} that could occur on a timescale of hours.

In detail, the synaptic modification works as follows (see Figures 1 and 2). The primary events for up- and downregulation are mediated by the NMDA receptors located at the postsynaptic membrane. The following scheme is chosen because both up- and downregulation depend on NMDA receptor activation (Markram, Roth, & Helmchen, 1998b; H. M., unpublished results). These receptors may be in three different states: the recovered state, N_{rec}, the state saturated with glutamate, N_u, and the state altered by intracellular calcium, N_d. The secondary messenger for up- and down-regulation may be in an active state, S_u and S_d, or an inactive state, $\bar{S}_u$ and $\bar{S}_d$, respectively. If a vesicle of neurotransmitter discharges, either spontaneously or due to a presynaptic action potential, glutamate is released and bound by postsynaptic NMDA receptors ($N_{rec} \rightarrow N_u$). Being in a state saturated by glutamate, the NMDA receptors will open when the postsynaptic membrane potential increases due to a backpropagating postsynaptic action potential, and this induces calcium flowing through NMDA channels into the postsynaptic cell. This calcium activates a secondary messenger ($\bar{S}_u \rightarrow S_u$), which diffuses to the presynaptic site and upregulates the probability of discharge ($\bar{P}^{\infty}_{dis} \rightarrow P^{\infty}_{dis}$). If, on the other hand, the postsynaptic membrane potential first increases due to a backpropagating action potential, voltage-activated calcium channels open; calcium flows in through these channels and binds to the NMDA receptors (Mayer, McDermott, Westbrook, Smith, & Barker,

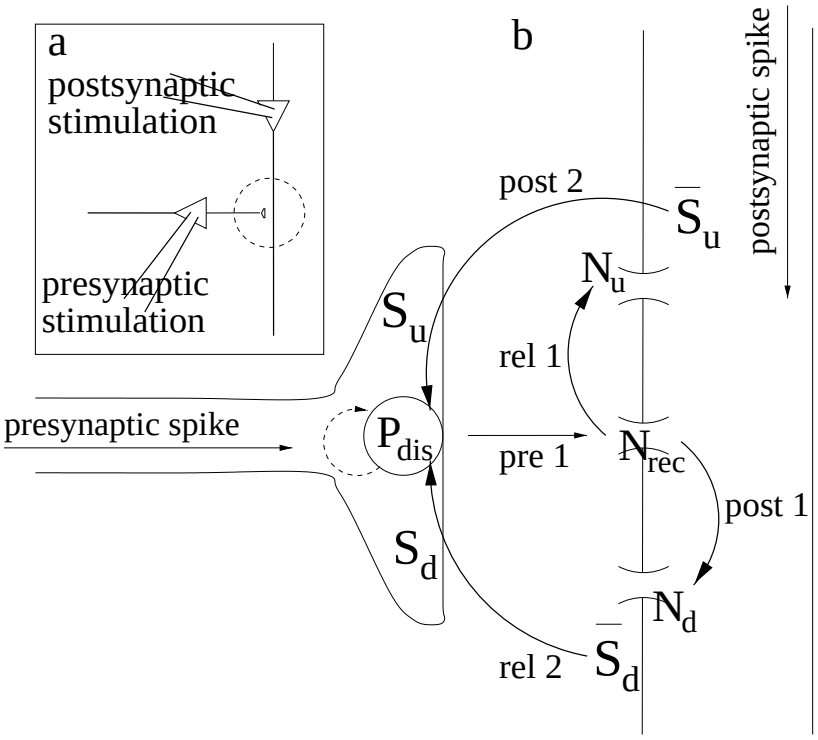

Figure 1: (a) Experimental arrangement. (b) Modification of P_{dis}. A vesicle at the site of release is discharged with probability P_{dis} (arrow pre1). Upregulation of P_{dis} requires a presynaptic release (vesicle discharge) followed by a postsynaptic spike (rel1, post2). Downregulation requires a postsynaptic spike followed by a presynaptic release (post1, rel2). N_u and N_d represent NMDA receptors in the up- and downregulating state, and S_u and S_d represent up- and downregulating secondary messenger, respectively.

1987), altering or redirecting their function ($N_{rec} \to N_d$). Subsequently released glutamate, which is triggered by a presynaptic action potential, now activates an altered NMDA receptor, and this leads to the activation of downregulating secondary messenger ($\bar{S}_d \to S_d$). This messenger diffuses back to the presynaptic location, and the probability of discharge is downregulated ($P^{\infty}_{dis} \to \bar{P}^{\infty}_{dis}$).

2.1 The Algorithm for Modifying the Discharge Probability. The above scenario can be summarized in the following "learning rule." Whenever a

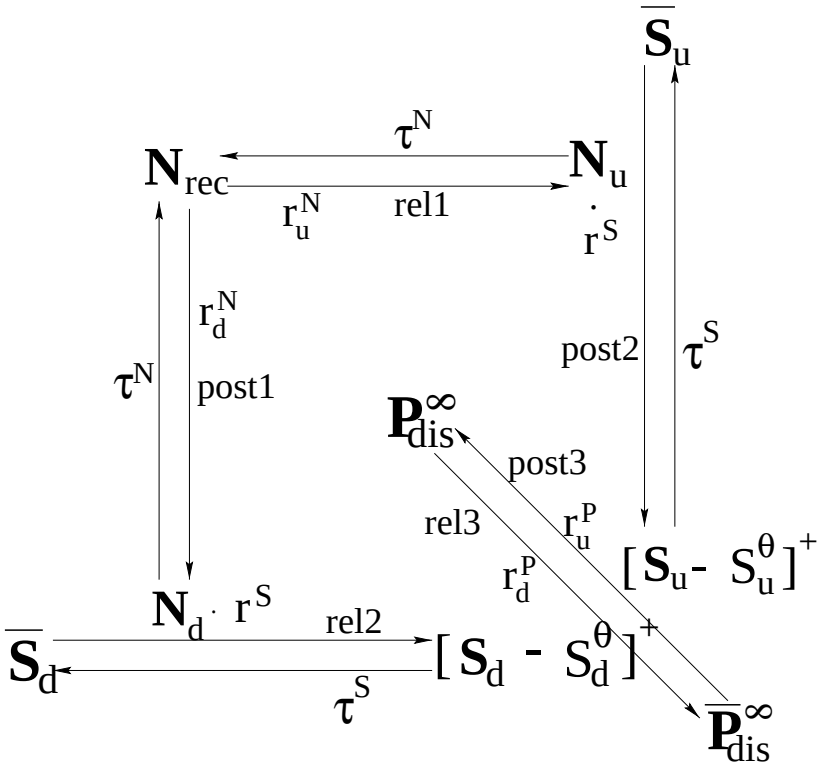

Figure 2: Kinetic scheme for modification of the limit probability of discharge, P_{dis}^∞. Upregulation of P_{dis}^∞ is mediated through the states N_u and S_u, while downregulation is mediated through the states N_d and S_d. These states decay naturally with time constants τ^N and τ^S, respectively. Transitions labeled with reli and posti ($i = 1, 2, 3$) occur instantaneously at either a *pre*synaptic release or at a postsynaptic spike. These instantaneous transitions are weighted by the factors written onto their arrows. For instance, at a postsynaptic spike, the state N_d is increased by $N_{rec} \cdot r_d^N$ (post1), and the state S_u is increased by $\bar{S}_u \cdot N_u \cdot r^S$ (post2). At a presynaptic release, for instance, P_{dis}^∞ is decreased by $r_d^P \cdot P_{dis}^\infty \cdot [S_d - S_d^\theta]^+$ (rel3).

postsynaptic action potential arrives at the synaptic site, three different processes are induced (indicated by post1–post3 in the scheme):

post1. The fraction r_d^N of N_{rec} is moved to N_d. This describes the altering of NMDA receptors due to calcium flowing into the postsynaptic site through voltage-activated channels.

post2. The fraction $r^S N_u$ of $\bar{S}_u$ is moved to S_u ($\bar{S}_u = 1 - S_u$). This describes the activation of upregulating secondary messenger proportional to the amount of receptors saturated with glutamate.

post3. The limit probability P_{dis}^{∞} is increased by $r_u^P \bar{P}_{dis}^{\infty} [S_u - S_u^{\theta}]^+$, where $\bar{P}_{dis}^{\infty} = 1 - P_{dis}^{\infty}$ and S_u^{θ} denotes the threshold to trigger upregulation ($[x]^+ = \max(x, 0)$). Thus, P_{dis}^{∞} is pushed toward 1 proportional to the amount of secondary messenger above threshold.

A release of a vesicle at the presynaptic site induces, completely symmetrically, the following three processes (indicated by rel1–rel3 in the scheme):

rel1. The fraction r_u^N of N_{rec} is moved to N_u. This describes the saturation of the recovered NMDA receptors with glutamate.

rel2. The fraction $r^S N_d$ of $\bar{S}_d$ is moved to S_d ($\bar{S}_d = 1 - S_d$). This describes the activation of downregulating the secondary messenger proportional to the amount of altered NMDA receptors.

rel3. The limit discharge probability is reduced by $r_d^P P_{dis}^{\infty} [S_d - S_d^{\theta}]^+$, that is, proportional to P_{dis}^{∞} and to the amount of S_d above threshold S_d^{θ}.

In a temporal order, up- and downregulation of P_{dis}^{∞} is each mediated by a primary and secondary event. The primary event for upregulation is a presynaptic release (rel1), and the secondary event is a postsynaptic spike (post2). The primary event for downregulation is a postsynaptic spike (post1), and the secondary event is a presynaptic release (rel2).

Beside these instantaneous transitions, the states N_u, N_d and S_u, S_d decay exponentially with the corresponding time constants τ^N and τ^S, respectively. In the diagram, these continuous transitions are represented by the arrows $N_u \xrightarrow{\tau^N} N_{rec}$, $N_d \xrightarrow{\tau^N} N_{rec}$ and $S_u \xrightarrow{\tau^S} \bar{S}_u$, and $S_d \xrightarrow{\tau^S} \bar{S}_d$, respectively. The convergence of P_{dis} to the limit probability P_{dis}^{∞} evolves with a modification time constant $\tau_M^P = 10$ min. (For a formulation of the kinetic scheme in terms of differential equations, see section A.1.)

2.2 The Model of Stochastic Release. Since on the presynaptic side the algorithm deals with release events, we modeled their generation by presynaptic spike events. This was done by two independent stochastic processes. First, a presynaptic action potential arriving at the synaptic bouton discharges a vesicle docked at the site of release with probability P_{dis}. Second, the probability that a vesicle is available at the site of release, P_v, is zero immediately after a vesicle discharge and recovers by a Poisson process with time constant $\tau_v^{rec} \approx 800$ms; that is, at any time step there is a small probability (proportional to $1/\tau_{rec}$) that the site of release will be reoccupied by a vesicle. The effective probability of release is given by the joint probability of the two stochastic processes, $P_{rel} = P_{dis} P_v$. Thus, to complete the algorithm, a presynaptic spike induces the following instantaneous transition

Table 1: Pseudocode for the Stochastic Synapse with Depression, Together with the Kinetic Scheme for Modifying P_{dis} (Figure 2).

```
for t=1 : dt : T
  if postsynaptic spike at t
    N_d = N_d + r_d^N N_rec
    S_u = S_u + r^S N_u (1 − S_u)
    P_dis^∞ = P_dis^∞ + r_u^P [S_u − S_u^θ]^+ (1 − P_dis^∞)
  end      % end of postsynaptic spike
  if presynaptic spike at t
    if vesicle_docked == 'yes'
      if random ≤ P_dis
        vesicle_docked = 'no'
        N_u = N_u + r_u^N N_rec
        S_d = S_d + r^S N_d (1 − S_d)
        P_dis^∞ = P_dis^∞ − r_d^P [S_d − S_d^θ]^+ P_dis^∞
      end      % end of vesicle discharge
    end      % end of discharge trial
  end      % end of presynaptic spike
  if random ≤ dt/τ_rec
    vesicle_docked = 'yes'
  end      % end of vesicle recovery
  S_u = S_u exp(−dt/τ^S),   S_d = S_d exp(−dt/τ^S)
  N_u = N_u exp(−dt/τ^N),   N_d = N_d exp(−dt/τ^N)
  N_rec = 1 − N_u − N_d
  P_dis = P_dis + dt/τ_M (P_dis^∞ − P_dis)
end      % end of simulation
```

Notes: The time step is set to $dt = 1$ ms, and the simulation time extends over T ms. The variable "random" represents a random number sampled from the uniform distribution between 0 and 1. The two sets of parameter values are given in the captions to Figure 3 and Figure 7.

(denoted by pre1 in Figure 1b):

pre1. If the site of release is occupied by a vesicle (which occurs with probability P_v), this vesicle is discharged by a presynaptic spike with probability P_{dis} and the site of release is cleared (setting $P_v = 0$).

Note that in accordance with the univesicular hypothesis (Triller & Korn, 1982), we assume that per release site, there is maximally one vesicle ready for release. The complete algorithm for synaptic modification and synaptic depression is compiled in a pseudocode in Table 1.

The vesicle depletion model described above is a stochastic version of the depressing synapse model introduced in Tsodyks and Markram (1997). Since the recovery is not instantaneous, a presynaptic spike following a previous discharge has less chance of encountering again a vesicle for discharging, and thus in the average the response appears to be depressed. To decide iteratively whether a presynaptic spike is successful, we introduce the probability P^n_{rel} that the nth presynaptic spike induces a release. Note that $P^n_{rel} = P_{dis}P^n_v$ is the product of the vesicle discharge probability and the probability of encountering a docked vesicle at the arrival of the nth spike. The probability of release for the $(n+1)$th spike is calculated to (cf. section A.2)

$$P^{n+1}_{rel} = P^n_{rel}(1 - P_{dis})\, e^{-\frac{\triangle_n}{\tau}} + P_{dis}(1 - e^{-\frac{\triangle_n}{\tau}}), \qquad \tau = \tau^{rec}_v, \tag{2.1}$$

where $\triangle_n = t^{sp,n+1}_{pre} - t^{sp,n}_{pre}$ is the time difference between the two presynaptic spikes and P_{dis} is the current value of the discharge probability. Averaged over different trials with the same stimulation protocol will give an average excitatory postsynaptic potential (EPSP) amplitude in response to the nth spike, which is proportional to P^n_{rel}. In Tsodyks and Markram (1997), this proportionality constant is called *absolute synaptic efficacy* (A), while in their mean-field model, the *use of synaptic efficacy* (U) describing the fraction of available transmitter discharged by a presynaptic spike corresponds to our discharge probability P_{dis}. In turn, the probability P_v of a vesicle's being docked at the site of release is interpreted as the fraction of transmitter available for release. In the mean-field model, the average is taken over several repetitions of the stimulation frequency or, equivalently, over several release sites in the same or different boutons for a single sample stimulus. Note that implicitly the univesicular hypothesis (per release site) is assumed since the full amount of discharged transmitter is missing immediately after a presynaptic spike, indicating that after discharge, no additional vesicles are ready for release. Our stochastic version may replicate the statistics of the nonaveraged responses during single trials of the synaptic stimulation experiments (cf. Tsodyks & Markram, 1997).

3 Results

3.1 Application of Specific Stimulation Protocols. The algorithm is based on dual whole-cell voltage recordings of neocortical pyramidal cells (Markram et al., 1997). It was tested against the following three experiments:

Experiment 1 (see Figure 3). Pre- and postsynaptic spike trains of 10 Hz and 5 spikes were paired with a lag of the presynaptic spikes of -10 and $+10$ms, respectively, repeated 10 times each 4 seconds. After pairing, the change in P_{dis} was recorded during the next 60 min. The increase in P^{∞}_{dis} for the 10 ms advanced presynaptic spikes and the decrease for the 10 ms

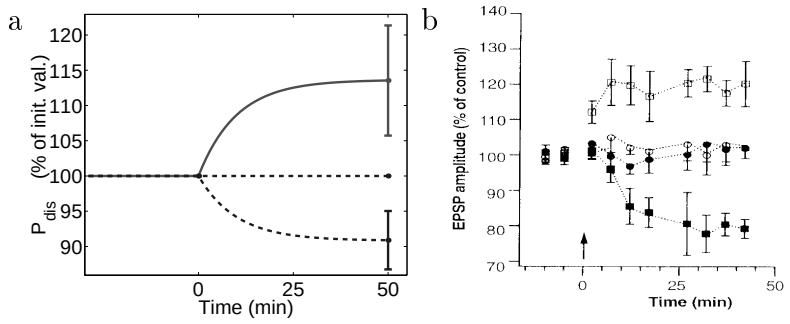

Figure 3: Experiment 1: Asymmetry of the synaptic modification. The evolution of P_{dis} toward P_{dis}^{∞} induced by pairing of 5 spikes at 10 Hz with a delay of the presynaptic spike train of -10 ms (upper trace) and 10 ms (lower trace). If the last presynaptic and the first postsynaptic spike were separated by 100 ms, no change occurs (middle traces). (a) Simulation results. The parameter values appearing in the scheme (see Figure 2) were chosen to fit the experimental data optimally. We set $r_u^N = 1$, $r_d^N = 0.5$, $\tau^N = 300$ ms, $r^S = 0.7$, $r_u^P = r_d^P = 0.1$, and $\tau^S = 600$ ms. The thresholds for the secondary messengers were set to $S_u^{\theta} = r^S$ and $S_d^{\theta} = r^N r^S$. As a starting value for the discharge probabilities, we used $P_{dis} = P_{dis}^{\infty} = 0.5$. (b) The same experiment in the slices. (Reprinted with permission from Markram et al., 1997.) Note that the change in P_{dis} (as shown in *a*) is proportional to the change in the EPSP amplitude of an isolated spike (as shown in *b*; cf. text). Vertical bars in *a* and *b* represent standard deviations.

retarded presynaptic spikes was faithfully reproduced by the algorithm. By translating the spike trains such that the last presynaptic spike was 100 ms apart of the first postsynaptic spike (and vice versa), no change occurred.

Experiment 2 (see Figure 4). Paired pre- and postsynaptic spikes trains of 5 spikes were triggered with a delay of the postsynaptic train of 2 ms, repeated 10 times each 4 seconds. The simulation was performed for different frequencies ranging from 2 to 40 Hz, and the final change in the probability of discharge, P_{dis}^{∞}, is evaluated. The main characteristics of the learning curve, the steep upstroke at 10 Hz, and the saturation at higher frequencies are well reproduced.

Experiment 3 (see Figure 5). Pre- and postsynaptic spike trains of 20 Hz were paired with a postsynaptic spike delay of 2 ms, repeated 10 times each 4 seconds. The number of spikes in the paired trains were varied from 2 up to 20, and for each number, P_{dis}^{∞} was determined. The surprising fact in this experiment was that the change in P_{dis}^{∞} did not accumulate but was neutralized by the following spikes. The simulations are compatible with these results and lay within the high standard deviations.

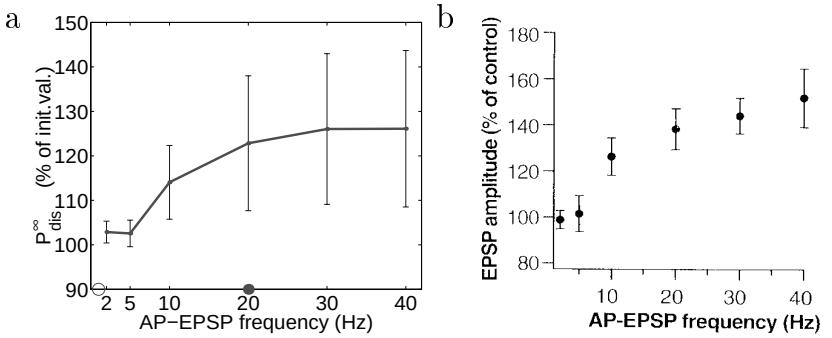

Figure 4: Experiment 2: Dependency on the frequency of the paired spike trains, each composed of 5 spikes. The change in P_{dis} shown 60 minutes after pairing of the spike trains with 2 ms delay of the postsynaptic train. In our model, the value of P_{dis} 60 minutes after pairing corresponds to P^{∞}_{dis} (cf. equation A.7). (a) Simulation results with the same parameter values as in Figure 3. The value at the dot (20 Hz) and the circle (1 Hz) should be compared with corresponding ones in Figures 5a, 6a, and 6b, respectively. (b) Same experiments in the slices. (Reprinted with permission from Markram et al., 1997.)

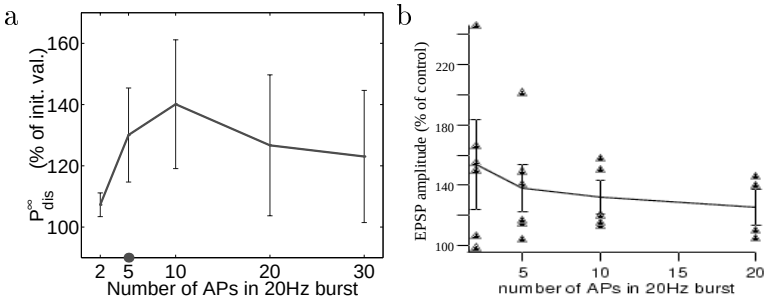

Figure 5: Experiment 3: Dependence on the number of spikes within the paired 20 Hz spike trains. (a) Simulation results with the same parameter values as in Figure 3. (b) Same experiments in the slices. The triangles show the outcome of the experiment with different pairs of cells (2 APs: n = 6; 5 APs: n = 6; 10 APs: n = 5; 20 APs: n = 4; n = number of different pairs).

The experimental data in Figures 3 through 5b show the changes in the amplitude of a first EPSP after a long period of silence. These changes could be induced by a change in either the absolute synaptic strength or the vesicle discharge probability. Inspecting the depression within a spike sequence, however, shows that after pairing, synapses with higher amplitude in the first EPSP are also more depressed in the responses to the subsequent spikes (data not shown). The time course of this depression is well predicted by

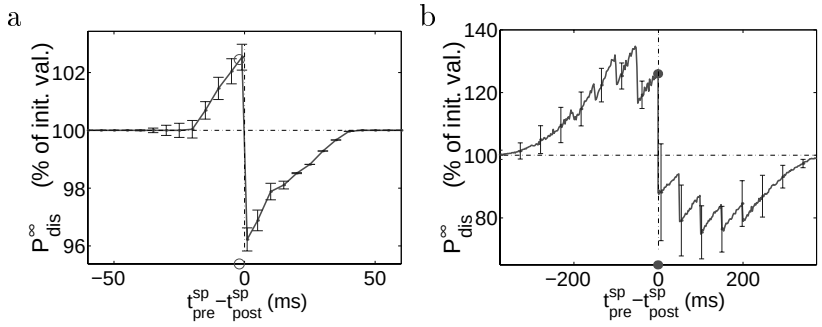

Figure 6: Change of P_{dis} versus interspike delays ($t^{sp}_{pre} - t^{sp}_{post}$). (a) In analogy to the experiment in Zhang et al. (1998), 50 paired spikes at 1 Hz were applied with a fixed presynaptic spike delay between −60 and 60 ms. The curve is qualitatively similar to the experimentally observed one, but due to the threshold effect, almost no change in P_{dis} is manifested (cf. Figures 4a and 4b evaluated at 1 Hz). (b) Pairing with the same number of spikes but now ordered in a 20 Hz train of 5 spikes with a fixed delay of the presynaptic spike train between −350 and 350ms, repeated 10 times, leads to a marked change in P_{dis} (note the different scales in *a* and *b*). Error bars drawn for selected points only.

formula 2.1 with a modified P_{dis} and a fixed proportionality constant. We therefore conclude that it is indeed P_{dis} that is subject to the long-term modification, and not the absolute synaptic strength.

What yet has to be tested for the cortical synapses in consideration is the change in P_{dis} for pre- and postsynaptic spike trains of a given frequency and varying delays. In other preparations, pairs of single pre- and postsynaptic spikes with frequency 1 Hz and various interspike delays were applied (Zhang et al., 1998; Bi & Poo, 1998). The same protocol applied to our model with parameter values used to fit experiments 1 through 3 yields a change in P_{dis} (see Figure 6a), which looks rather close to the change in the synaptic strength observed in Bi and Poo's experiments and matches well the width of the modification window. However, the size of the induced changes is much smaller than that seen in their experiment. In our simulation, we had to introduce thresholds precisely to exclude too much upregulation at a low stimulation frequency (see Figure 3). Cortical synapses seem to be protected against modifications induced by single pairs of spikes as long as these pairs arrive less frequently than 5 Hz. Such a protection mechanism would make sense in stabilizing memory (Fusi, Annunziato, Badoni, Salamon, & Amit, 2000).

If the same number of paired spikes with the same relative delay as in the experiment is applied to our cortical synapse model with a frequency higher than 5 Hz, a considerable change is evoked. The time constant with which the repetitive stimulations are integrated is determined by the time constant

of the secondary messenger τ^S, while the width of the learning window itself is determined by the time constant of the NMDA receptors τ^N, each corrected by the threshold effect. Figure 6b shows the relative change in P^∞_{dis} for spike trains of 5 spikes at 20 Hz with different delays of the presynaptic train with respect to the postsynaptic one. The five peaks in the upper and lower branch are each due to the partial synchrony induced by a full shift of an interspike interval. For a delay below -200 ms and above $+200$ ms, the spike patterns do not interfere anymore, and the smoothly decaying branches represent the effective window of modification. Notice that downregulation is maximal at a delay of 100 ms of the presynaptic spike train, while upregulation is maximal at a delay of -50 ms. The minimum at 100 ms (instead of 1 ms) delay is explained by the fact that at a postsynaptic spike, only the fraction r^N_d of N_{rec} is moved to N_d. In turn, the maximum at -50 ms (instead of -1 ms) delay is explained by the fact that not each presynaptic spike induces a neurotransmitter release. The singularity in our simulation at zero delay is an artifact of our simplified model, which assumes instantaneous changes in the kinetic scheme. Depending on the true time course of the reactions in the scheme, the singularity will smooth out, and the zero change of P^∞_{dis} may appear at either a positive or a negative delay.

It is interesting to note that our cortical synapse model would reproduce the same size of the synaptic change as in the cited experiments if not 50 but 500 paired spikes at 1 Hz are applied. The reason is that for frequencies below 5 Hz, the induced changes in P^∞_{dis} add nearly linearly with the number of paired action potentials. This is not true anymore for a frequency of 20 Hz, as revealed by experiment 3 (see Figure 5).

3.2 Application of Poisson Spike Trains. Next we investigate the average behavior of our spike-based learning rule when applying nonstationary Poisson spike trains. In this case, the kinetic scheme can be translated directly into differential equations with time-varying coefficients. Following the diagonal arrows in the scheme, P^∞_{dis} is upregulated at each postsynaptic spike proportionally to $(1 - P^\infty_{dis})\,[S_u - S^\theta_u]^+$ and downregulated at each presynaptic release proportionally to $P^\infty_{dis}\,[S_d - S^\theta_d]^+$, where $[x]^+ = \max\{x, 0\}$. If we denote the presynaptic release and postsynaptic spike frequency by f^{rel}_{pre} and f^{sp}_{post}, respectively, the expected change of P^∞_{dis} at time t is obtained from the kinetic scheme according to

$$\frac{dP^\infty_{dis}}{dt} = r^P_u(1 - P^\infty_{dis})\,[S^+_u - S^\theta_u]^+ f^{sp}_{post} - r^P_d P^\infty_{dis}\,[S^+_d - S^\theta_d]^+ f^{rel}_{pre}, \tag{3.1}$$

where S^+_u and S^+_d represent the expectation values of the secondary messengers for up- and downregulation immediately after a post- and presynaptic spike, respectively (cf. sections A.1–A.3). Such an expectation value corresponds to the average over a population of identical synapses with the same instantaneous spike statistics. If the secondary messenger has a time

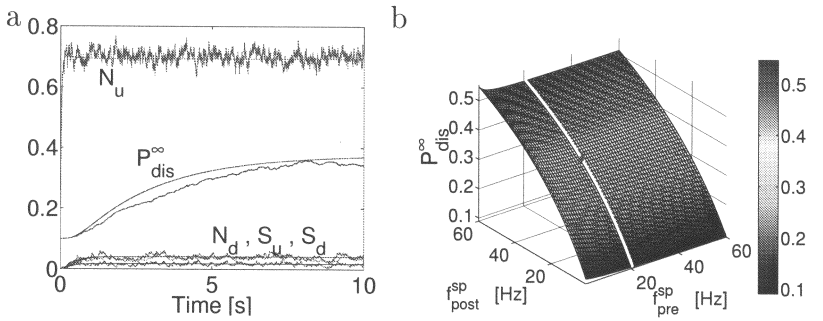

Figure 7: (a) Convergence to the steady states of N_u, N_d, S_u, S_d, and P^{∞}_{dis} from the starting values 0 and 0.1, respectively. The applied Poisson frequencies were fixed to $f^{sp}_{pre} = 20$ and $f^{sp}_{post} = 30$ Hz. The noisy curves represent an average over 100 trials (of the algorithm in Table 1) while the smooth lines represent the mean-field solutions (obtained by integrating the differential equations, equations A.1–A.8). (b) For each pre- and postsynaptic Poisson spike frequency, there is a unique steady state for $P^{\infty}_{dis} = P_{dis}$ (plot of equation A.16). The sensitivity to f^{sp}_{post} is mainly due to the higher-order term in f^{sp}_{post}, and the insensitivity to f^{sp}_{pre} is due to the synaptic depression. The white curve shows P^{∞}_{dis} restricted to $f^{sp}_{pre} = 20$ Hz, and the dot on this curve corresponds to $f^{sp}_{post} = 30$ Hz with a discharge probability of $P^{\infty}_{dis} \approx 0.37$ (cf. left panel). The insensitivity in f^{sp}_{pre} is explained by the synaptic depression, and the sensitivity in f^{sp}_{post} is mainly due to the higher-order term in f^{sp}_{post}. The parameters were $\tau^N_u = \tau^N_d = 100$ ms, $\tau^S_u = \tau^S_d = 800$ ms, $r^N_u = r^N_d = 0.8$, $r^S = 0.4$, $r^P_u = 0.1$, $r^P_d = 1$, $S^{\theta}_u = S^{\theta}_d = 0$.

constant large enough to integrate the signals, it will be itself roughly proportional to the first-order correlation $f^{rel}_{pre} f^{sp}_{post}$. Neglecting the thresholds S^{θ}, the first term in equation 3.1 then is of order $f^{rel}_{pre}(f^{sp}_{post})^2$, and the second term is of order $f^{sp}_{post}(f^{rel}_{pre})^2$. It is this higher-order nonlinearity that keeps the synapse sensitive not only to spike correlations but also to average firing rates. For stationary Poisson trains, P^{∞}_{dis} converges to a unique steady state (see Figure 7a and equation A.16), which is increasing with respect to f^{sp}_{post} and weakly decreasing with respect to f^{sp}_{pre} and f^{rel}_{pre}, respectively (see Figure 7b). In this section we preferred to choose a simpler parameter setting with vanishing thresholds and that is symmetric with the exception of the rates for up- and downregulation. In order to obtain the anti-Hebbian regime at low postsynaptic frequencies in the BCM rule, a high-ratio $\frac{r^P_d}{r^P_u}$ is necessary.

In the following we modulate the Poisson spike frequencies and impose additional spike-by-spike correlations. We consider three scenarios, each of

which reveals a particular aspect of our learning rule:

1. A jump in the postsynaptic spike frequency leads to an adaptation of P_{dis}^{∞} similar to the synaptic weight adaptation in the BCM theory.
2. Modulating sinusoidally the pre- and postsynaptic frequencies with a fixed phase lag leads to an adaptation of P_{dis}^{∞} reminiscent of a Hebbian-anti-Hebbian rule.
3. Introducing spike-by-spike correlations within the pre- and postsynaptic spike trains (while keeping their frequencies fixed) leads to an adaptation of P_{dis}^{∞} depending on the relative spike timing.

3.2.1 Comparison with the BCM Rule. The BCM theory was developed to explain the synaptic modifications in the visual cortex of cats observed under various rearing conditions (for a review, see Bear, Cooper, & Ebner, 1987). In the monocular deprivation experiment, a cortical cell that initially dominantly responded to the deprived eye is shown to shift its dominance slowly to the untouched eye. In BCM theory, this is explained by a sliding threshold for the postsynaptic activity, θ_M, which determines whether the synaptic strengths are down- or upregulated. After suturing the dominant eye, the preferred stimulus may only subcritically excite the postsynaptic cell, and the strengths of the activated synapses are downregulated. To gain the sensitivity to an activity pattern from the unsutured eye, the modification threshold θ_M slowly decays until the postsynaptic activity becomes supercritical, and the synapses from the untouched eye are now strengthened and finally dominate the cell's firing behavior. In our context, the synaptic modification may be written as

$$\frac{dP_{dis}^{\infty}}{dt} = r_u^P \, \phi(f_{post}^{sp}) \, f_{pre}^{rel} \,, \tag{3.2}$$

where ϕ, as a function of the postsynaptic activity, satisfies the BCM properties $\phi(0) = \phi(\theta_M) = 0$ and $\phi(f_{post}^{sp}) \leq 0$ if $f_{post}^{sp} \leq \theta_M$ and $\phi(f_{post}^{sp}) > 0$ if $f_{post}^{sp} > \theta_M$ (see Figure 8b). Note that unlike the BCM theory, where the ϕ is only a function of the postsynaptic rate, it depends on the individual synapse in our case. Distinguishing between the f_{post}-dependency of ϕ on a fast and slow timescale leads to the sliding threshold property. Taking into account the transfer from the presynaptic frequencies to the postsynaptic response, this is an important means of the synapses to keep the postsynaptic activity around a point of the cell's maximal sensitivity. If after reaching steady-state values, the postsynaptic frequency drops, say, by artificially reducing the input from the dominant eye, P_{dis}^{∞} of the activated synapses is slowly downregulated (see Figure 8a). The rate of the change in P_{dis}^{∞} and its final value are shown in Figure 8b as a function of the new value of f_{post}^{sp}. The modulation threshold θ_M at which up- and downregulating forces neutralize is implicitly driven by the running mean of the postsynaptic spike

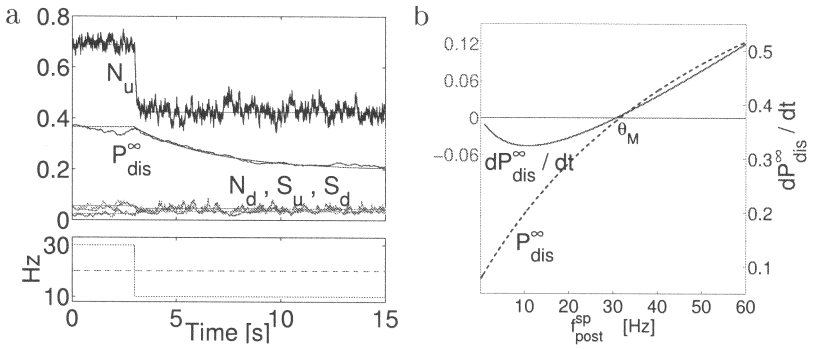

Figure 8: BCM rule. (a) After converging to the steady state for $f^{sp}_{pre} = 20$ and $f^{sp}_{post} = 30$ Hz, an instantaneous jump of the postsynaptic frequency to 10 Hz will downregulate P^{∞}_{dis}. Noisy lines represent the average over 50 trials (of the algorithm in Table 1) while the smooth lines represent the mean-field solutions (obtained by integrating the differential equations, A.1–A.8). (b) Starting at the same steady state as in *a*, the vesicle discharge probability increases if the postsynaptic spike frequency jumps above θ_M (= 30 Hz) and decreases if it jumps below. The rate of the change is a nonmonotonic function of the new value of f^{sp}_{post} (solid line, calculated according to equation 3.2 and section A.4 with $f^{sp}_{pre} = 20$ Hz). The dashed curve shows the new value of P^{∞}_{dis} after reaching the steady state and corresponds to the white curve in Figure 7b.

frequency. Keeping the spike frequencies fixed at the new value, the synaptic parameters will adapt such that f^{sp}_{post} becomes a zero of ϕ and therefore $\theta_M = f^{sp}_{post}$ (cf. Section A.4 for an analytical treatment). At this point a slight change in the postsynaptic average frequency will result in a corresponding change of the vesicle discharge probability. A new presynaptic activation pattern, say, generated by stimulating the unsutured eye, sharing the same synapses will now have the chance for growing influence onto the postsynaptic cell, and the average postsynaptic activity would start to increase again. A more detailed discussion of the learning rule's selection and stabilization properties to dominant input patterns is given in Kempter et al. (1999b) and Abbott and Song (1999). Let us finally mention that it is possible to retrieve the rule of Artola-Bröcker-Singer (Artola & Singer, 1993), which differs from the BCM rule by an additional threshold below which no modification takes place. In our scheme this is achieved by setting both thresholds S^{θ}_{u} and S^{θ}_{d} to positive values.

3.2.2 A Generalized Asymmetric Hebbian Rule. Different forms of Hebbian learning rules have been investigated that consider the product of pre- and postsynaptic activities as the quantity determining the synaptic mod-

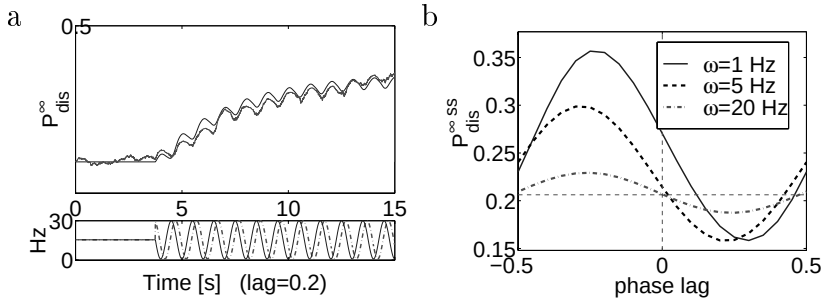

Figure 9: (a) Sinusoidal modulation of f^{sp}_{pre} (full line in the lower panel) and f^{sp}_{post} (dashed line in the lower panel) of $\omega = 1$ Hz with presynaptic phase lag of 0.2 induces upregulation of P^{∞}_{dis} (upper panel). The noisy line in the upper panel represents the average time evolution of P^{∞}_{dis} over 100 trials (of the algorithm in Table 1) and the dashed curve represents the mean-field solution (of equations A.1–A.8). (b) Steady-state values of P_{dis} for sinusoidal modulations of the pre- and postsynaptic frequencies versus presynaptic phase lag. The modulation frequencies were $\omega = 1,\ 5,\ 20$ Hz. Note that the curves represent smoothed versions of the learning curves shown in Figure 6. For the 1 Hz modulation, the synaptic depression may advance the release activity with respect to the presynaptic spike activity, and P^{∞}_{dis} may be upregulated even if this lags the postsynaptic peak activity. The horizontal dashed line represents the steady state without modulation. Same parameter values as in the caption of Figure 7.

ification (see, e.g., Brown & Chatterji, 1994, for a review). To prevent the saturation of the synaptic strengths, mixtures of Hebbian and anti-Hebbian rules are proposed by focusing on the covariance between pre- and postsynaptic activities (Sejnowski, 1977) or by normalization of the synaptic weight (Oja, 1982). The learning rule we consider belongs to the same class of Hebbian mixtures, however, with a strong asymmetry in the temporal correlations. This asymmetry makes the synapse sensitive to the phase lag between modulations of the pre- and postsynaptic frequencies. If the postsynaptic spike activity lags, the presynaptic release activity, P^{∞}_{dis}, is upregulated, and if the postsynaptic spike activity leads the presynaptic release activity, P^{∞}_{dis} is downregulated. Figure 9a shows the change of P^{∞}_{dis} for a sinusoidal modulation of the pre- and postsynaptic spike frequencies of 1 Hz and phase lag of 0.2. The steady state of P^{∞}_{dis} for different rates of modulation and different lags is shown in Figure 9b. Two things are worth emphasizing. First, for slow modulation rates in the range of the vesicle recovery time constant, the point of zero change appears at positive lag of the presynaptic activity. This is rather counterintuitive since at positive lag, downregulation would be expected. Second, the maximal changes appear at lags of $\pm\frac{1}{4}$ independent of frequency of modulation. This is true even if the pe-

riod of the modulation is much larger than the time window of synaptic adaptation.

To gain insight into these mechanisms, we constrain ourselves to the simplifying assumption of an instantaneous recovery of the secondary messenger ($\tau^S = 0$). This assumption implies that the amount of activated secondary messenger S_u and S_d is always proportional to the NMDA receptors in the states N_u and N_d, respectively. On the other hand, if the pre- and postsynaptic spikes are independent, these states are roughly proportional to the running mean of the previous presynaptic release and postsynaptic spike frequencies, respectively (which follows from integrating equations A.1 and A.2). If we, moreover, neglect the thresholds for up- and downregulation ($S_u^\theta = S_d^\theta = 0$), then formula 3.1 for the synaptic modification can be comprised by the generalized asymmetric Hebbian rule

$$\frac{dP_{dis}^{\infty}}{dt} \approx r_u^P (1 - P_{dis}^{\infty}) \langle f_{pre}^{rel} \rangle f_{post}^{sp} - r_d^P P_{dis}^{\infty} \langle f_{post}^{sp} \rangle f_{pre}^{rel}, \tag{3.3}$$

where

$$\langle f \rangle = \frac{1}{\tau^N} \int_0^\infty f(t - t') e^{-t'/\tau^N} \, dt'$$

represents the running mean of f. Note that by the setting $\tau^S = 0$, the third-order nonlinearity in equation 3.1 is reduced to the usual correlations, although with the presynaptic release instead of the presynaptic spike frequency. The transformation of the presynaptic spike to the presynaptic release frequency itself is governed by the dynamics of the vesicle recovery (cf. equations A.8 and A.9). If we assume an instantaneous vesicle recovery ($\tau_v^{rec} = 0$), there is no activity-dependent depression, and the presynaptic release rate is proportional to the presynaptic spike rate. For "static" synapses, f_{pre}^{rel} can therefore be replaced by f_{pre}^{sp} in equation 3.3.

Equation 3.3 provides an explanation of Figure 9. First, we observe that averaging f over the past delays the averaged quantity $\langle f \rangle$. Second, we note that the effect of the synaptic depression is to advance the release rate f_{pre}^{rel} compared to the spike rate f_{pre}^{sp} (since the peak of the release rate is depressed; see, e.g., Abbott, Varela, Sen, & Nelson, 1997). For lag zero and a modulation frequency of $\omega = 1$ Hz these two effects cancel, and the factors in the Hebbian part of equation 3.3 are correlated, but not the ones in the anti-Hebbian part. This explains the upregulation of P_{dis} even at a small, positive lag of the presynaptic spike activity (see Figure 9b). For higher modulation frequencies beyond the time constant of vesicle recovery, however, the phase advance vanishes, and at zero lag, the Hebbian and anti-Hebbian part in equation 3.3 cancel each other. The maximal upregulation is reached for a presynaptic phase advance of $\frac{1}{4}$ since due to the delaying effect of averaging, this leads to correlated factors in the Hebbian part of equation 3.3 and to uncorrelated factors in the anti-Hebbian part. Similarly,

maximal downregulation of P_{dis} is obtained around a presynaptic phase lag of $-\frac{1}{4}$, and this barely depends on the modulation frequency.

3.2.3 A Spike Correlation Rule. In the previous paragraph, we considered correlations between pre- and postsynaptic mean firing rates. Independent of these correlations, the pre- and postsynaptic spike trains may exhibit spike-by-spike correlations that affect the synaptic efficacy as well. To quantify the influence of this microcorrelation, we introduce the notion of (first-order) spike correlation between pre- and postsynaptic spike train. This measure describes the temporal asymmetry with which on the average, a presynaptic spike occurs between the last previous and the next following postsynaptic spike. For a given presynaptic spike time t_{pre}, we denote the time of the previous postsynaptic spike by $t^<_{post}$ and the time of the following postsynaptic spike by $t^>_{post}$. The spike correlation c_s is then defined by

$$c_s := \frac{1}{\triangle}\left(\langle t_{pre} - t^<_{post}\rangle_{t_{pre}} - \langle t^>_{post} - t_{pre}\rangle_{t_{pre}}\right),$$

with normalization $\triangle = \langle t_{pre} - t^<_{post}\rangle_{t_{pre}} + \langle t^>_{post} - t_{pre}\rangle_{t_{pre}}$. Due to the normalization, c_s is restricted to values between -1 and 1, and these boundary values are reached if the presynaptic spikes all occur either instantaneously after or before the postsynaptic ones, respectively. Hence, we characterize the pre- and postsynaptic spike trains by three numbers, their (instantaneous) frequencies and their spike correlation, f^{sp}_{pre}, f^{sp}_{post}, and c_s. Although there is no surprise that the sign of the synaptic change will correspond to the sign of the correlation c_s imposed to the spike trains, it is important on a formal level to quantify the synaptic modification as a function of these three variables. The computational power of rate-based neurons with transfer functions depending on the presynaptic correlations was recently characterized (Maass, 1998), but learning algorithms for such networks have yet to be studied.

Let us now assume a scenario where the pre- and postsynaptic spike trains each exhibit Poisson characteristics when considered by themselves, but when compared to each other, they show some spike correlation $c_s \in [-1, 1]$. Figure 10a depicts the change of P^∞_{dis} when after 2 seconds of Poisson stimulation, the spike correlation c_s jumps from 0 to 1 (first pre-, then post-) and from 0 to -1 (first post-, then pre-), respectively. Figure 10b shows the steady state of P^∞_{dis} as a function of c_s for fixed pre- and post-synaptic frequencies. Reordering the left and right branches (inset of the figure) yields an average modification similar to the one induced by the shift between the periodic pre- and postsynaptic spike trains in Figure 6.

To explain the effect of the spike correlation, we again assume the simplified setting of an instantaneous recovery of the secondary messenger ($\tau^S = 0$) and of vanishing thresholds S^θ_u and S^θ_d. The spike correlation implicitly determines the distribution of the NMDA receptors over the states N_{rec}, N_u, and N_d. If c_s is negative, the transition $N_{rec} \to N_u$ induced by a

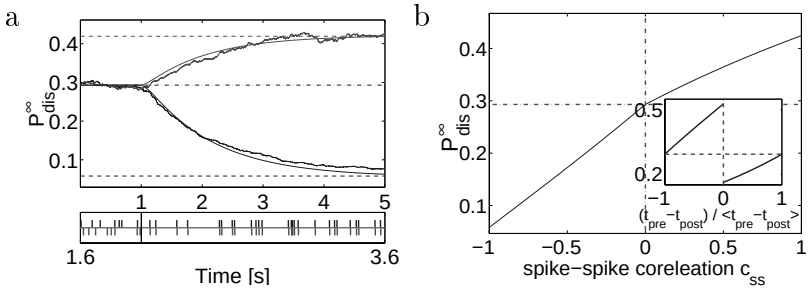

Figure 10: (a) Upper panel: After reaching the steady state for a pre- and postsynaptic Poisson spike train of 20 Hz (0–2 sec), the spike correlation c_s was switched from either 0 to 1 (inducing an increase of P^{∞}_{dis}) or 0 to -1 (inducing a decrease of P^{∞}_{dis}). The noisy lines represent the average for 100 repetitions of the experiment, and the smooth lines represent empirically corrected mean-field calculations (cf. section A.5). Lower panel: After switching c_s from 0 to 1, the spikes of the postsynaptic neuron (lower trace) were elicited immediately after a presynaptic spike (upper trace). (b) Change of P^{∞}_{dis} according to equation 3.4 for $f^{sp}_{pre} = 20$ Hz and $f^{sp}_{post} = 30$ Hz versus the spike correlations c_s. The inset shows a reordering of the branches and essentially reflects the steady state of P^{∞}_{dis} as a function of the (normalized and averaged) spike time differences $t^{sp}_{pre} - t^{sp}_{post}$. Same parameter values as in the caption of Figure 7.

presynaptic release is less effective since with high probability, an immediately preceding transition $N_{rec} \to N_d$ induced by a postsynaptic spike reduced the state N_{rec}. Since N_u tunes through the postsynaptic frequency, the upregulation of P^{∞}_{dis}, the net increase of P^{∞}_{dis} is reduced. In turn, a positive c_s unfavors the state N_d since a previously arrived presynaptic spike triggered with probability P_{rel} the transition $N_{rec} \to N_u$ and less is remaining in the state N_{rec} to be moved to N_d. In this case the downregulation of P^{∞}_{dis} is less effective. This reasoning can be expressed by adapting formula 3.3 to

$$\begin{aligned}\frac{dP^{\infty}_{dis}}{dt} \approx\ & r^P_u(1 - P^{\infty}_{dis})\langle f^{rel}_{pre}(1 - r^N_d[-c_s]^+)\rangle f^{sp}_{post} \\ & - r^P_d P^{\infty}_{dis}\langle f^{sp}_{post}(1 - r^N_u[c_s]^+ P_{rel})\rangle f^{rel}_{pre}\,. \end{aligned} \tag{3.4}$$

Note again that the presynaptic release frequency corresponds to the presynaptic spike frequency times the probability of vesicle release, $f^{rel}_{pre} = f^{sp}_{pre} P_{rel}$, and that the latter itself depends on the dynamics of the presynaptic spike frequency (see equation 2.1 and section A.2). Equations 3.3 and 3.4 represent an asymmetric version of the traditional covariance rule based on mean firing rates (see, e.g., Sejnowski, 1977) with an account of correlations on the level of spikes rather than only on the level of the frequencies.

3.3 Full versus Simplified Model. One may ask whether the simplified model explaining the mean-field properties in sections 3.2.2 and 3.2.3 above is sufficient to reproduce the experimental results. As long as one is interested in modeling the temporal asymmetry of the synaptic modification, this is indeed true, but it is difficult to fit the nonlinearities of the additional experiments. To recapitulate, the simplified model is obtained by neglecting the dynamics of the secondary messenger, formally by taking the limit $\tau^S = 0$ with $r^S = 1$. (In this case, one may skip the steps post2 and rel2 in the algorithm and directly use the quantities N_u, N_d for S_u, S_d in the steps post3 and rel3, respectively. Similarly, in the mean-field description, equation 3.1, one may identify S_u^+, S_d^+ with N_u, N_d, respectively (see section A.3). In a rough simplification, the discharge probability is then upregulated at each postsynaptic spike, depending on the running mean of the presynaptic release rate, and downregulated at each presynaptic release, depending on the running mean of the postsynaptic spike rate,

$$\triangle P_{dis} \approx \langle f_{pre}^{rel} \rangle f_{post}^{sp} - \langle f_{post}^{sp} \rangle f_{pre}^{rel}. \tag{3.5}$$

This form of the algorithm would represent the minimal model to reproduce the temporal asymmetries in the Figures 3, 6, and 10a, but also in Figure 9b reflecting the phase-advance property of depressing synapses. If the rule is applied to the strength of nondepressing synapses, it would probably also be sufficient to reproduce the experiments in other preparations, which were confined to investigate the asymmetry of the learning window at a fixed frequency of the pairing (Bell et al., 1997; Zhang et al., 1998; Bi & Poo, 1998). In our case of depressing synapses, however, we did not to succeed in matching at the same time the additional experiments 2 and 3 with their nonlinear increase as a function of the pairing frequency and the nonmonotonic change as a function of the number of spikes. These two experiments let us introduce the S-variable in the kinetic scheme as well as the third-order nonlinearity given by the steps post3 and rel3 (which are established by the delta function in Equation A.5).

First, two different time constants are needed to model: (1) the width of the learning window, which is probably narrower than 50 ms, as seen in Figures 3 and 6a, and (2) the cumulating effect of the spike pairing repeated in steps of 100 ms, as shown by the steep increase at 10 Hz in Figure 4. Experiment 3 also suggests that a time constant larger than 50 ms is involved since a transient behavior is seen extending over the 500 ms of the first 10 to 15 spikes of 20 Hz (see Figure 5). The choice of two different secondary messengers was guided by the simplicity of the resulting scheme, and we do not make any statement about their nature. In fact, one could think of a single type of secondary messenger, but in this case additional processes have to be modeled to read out from this messenger whether and how much the discharge probability should be up- or downregulated (Grzywacz & Burgi, 1998).

Second, we introduced the third-order nonlinearity since in the presence of synaptic depression, it was difficult to obtain a nonlinear increase of the learning curve with respect to increasing frequencies (see Figure 4). The reason is that increasing the pairing frequency is essentially balanced out on the right-hand side of equation 3.5. If we consider the full scheme with large τ^S (compared to $1/f$), however, equation 3.5 turns into

$$\triangle P_{dis} \approx \langle f_{pre}^{rel} \rangle_N \langle f_{post}^{sp} \rangle_S f_{post}^{sp} - \langle f_{post}^{sp} \rangle_N \langle f_{pre}^{rel} \rangle_S f_{pre}^{rel}, \tag{3.6}$$

where $\langle . \rangle_N$ and $\langle . \rangle_S$ denote the running mean with time constants τ^N and τ^S, respectively (cf. equation 3.3 and section A.3). Now f_{post}^{sp} arises in the square in the first term, which gives the steep increase with the pairing frequency. Importantly, f_{pre}^{rel}, which arises in the square in the second term, remains in the order of 1 Hz due to the synaptic depression (cf. section A.2). Although this reasoning deals with Poisson rates, the problem that the synaptic change is largely indifferent to increasing frequencies if we wouldn't introduce further nonlinearities is also seen in experiment 2. At medium frequencies, in a train of five paired spikes, one of the first and often the last presynaptic spike only triggers a release. In this case, the postsynaptic spikes in the middle of the train are placed symmetrically after and before a presynaptic release, and no clear dominance for upregulation is shown. For higher frequencies, the duration of the 5-spike train is markedly below the vesicle recovery time constant, and maximally one release can be triggered. Due to the stochastic nature, this release may arise in response to the second presynaptic spike, and by the preceded postsynaptic event downregulation is favored. Moreover, since in this case the first postsynaptic spike depleted the common pool (N_{rec}), the same release event will be much less effective in inducing an upregulation via immediately following postsynaptic spike.

4 Discussion

4.1 Summary. We presented an algorithm that allows the prediction of the change in the temporal dynamics of synaptic transmission by depressing synapses induced by arbitrary trains of pre- and postsynaptic action potentials. The algorithm is based on the importance of precise relative timing of the pre- and postsynaptic action potentials and therefore constitutes a novel form of learning algorithm. It reproduces the change in the synaptic responses induced by the pairing: the asymmetry with respect to the spike-time difference, the monotonic increase with respect to the frequency, and the nonmonotonic dependency on the number of paired spikes.

When applying Poisson spike trains, an anti-Hebbian regime is followed by a Hebbian regime during an increase of the postsynaptic frequency, provided the relative degree of upregulation (r_u^P / r_d^P) is small enough. This feature, together with the slow adaptation of the borderline between the two regimes, allows the rule to preserve the stability and the selectivity to new

patterns as described by the BCM theory. When modulating the pre- and postsynaptic spike frequencies, the synaptic dynamics may dominate the temporal asymmetry of the learning rule, and, surprisingly, upregulation of the discharge probability may occur even if the presynaptic peak activity lags the postsynaptic peak activity. Finally, quantifying the spike correlation within two arbitrary spike trains permits specifying the learning rule as a function of the instantaneous pre- and postsynaptic frequencies and their instantaneous spike correlation. Such a formulation fits into the recently proposed framework of generalized neural networks, which are processing average firing rate together with average spike correlations (Maass, 1998).

4.2 Experimental Basis for the Model. The algorithm was constructed under several experimental constraints:

1. Excitatory glutamatergic synapses between pyramidal neurons in the neocortex are fast-depressing synapses, and the change that follows Hebbian pairing is equivalent to a change in the discharge probability P_{dis} (Markram & Tsodyks, 1996). This change alters the temporal dynamics of transmission (Tsodyks & Markram, 1997; Abbott et al., 1997).

2. The asymmetrical modification window with respect to relative timing of pre- and postsynaptic action potentials, as reported by Markram et al. (1997), was considered. In this window, up- and downregulation fall in a window of around 100 ms after and before a postsynaptic action potential, respectively.

3. Upregulation is dependent on NMDA receptors, and the backpropagating action potential can cause rapid pulses of Ca^{2+} through the NMDA receptor (Markram, Roth, & Helmchen, 1998; Spruston, Jonas, & Sakmann, 1995). The speed of these AP-evoked Ca^{2+} concentration pulses via NMDA receptors is such that only an enzyme with very high forward binding rates could capture this Ca^{2+}, providing the ideal situation for a coincident detector protein (Markram, Roth, & Helmchen, 1998). We therefore propose that the amplitude of the upregulation follows a time course of the NMDA current, which has a rise time constant of 10 to 20 ms and a decay time constant of 100 to 300 ms (Jonas & Spruston, 1994). The time constant of approximatively 60 ms for upregulation observed experimentally could be due to a threshold effect.

4. The magnitude of the upregulation increases as a function of the frequency of the pre- and postsynaptic action potentials in the train with an onset between 5 and 10 Hz (Markram et al., 1997).

5. Surprisingly, the upregulation was not increased when more action potentials were included in a train of a given frequency (data included in this study). This is proposed to be due to the balanced effects of up- and downregulation, which, after an initial transient, are reached for the given train of action potentials.

6. Downregulation is also dependent on NMDA receptor activation and on Ca^{2+} influx (HM, unpublished data). We therefore propose that the rise in

Ca^{2+} concentration following a backpropagating action potential influences the NMDA receptor in such a manner that it results in downregulation when activated. Indeed, the dendritic Ca^{2+} transient has a similar time course as that of downregulation (Markram, Helm, & Sakmann, 1995), and intracellular Ca^{2+} has been shown to modify the kinetics of the NMDA receptor (Mayer et al., 1987; Medina, Filippova, Bakhramov, & Bregestovski, 1996; Mayer, 1998; Antonov, Gmiro, & Johnson, 1998).

7. Ca^{2+} from different sources or modes of influx can activate different processes due to differential binding as a function of forward and backward rate constants (Markram, Roth, & Helmchen, 1998).

4.3 Comparison with Other Learning Rules. Asymmetric learning rules based on mean firing rates or individual spike times were investigated in different contexts. They were used for storing trajectories (Abbott, 1996), modeling hippocampal place fields of rats wandering around in the Morris water maze (Blum & Abbott, 1996; Gerstner & Abbott, 1997), and modeling the temporal selectivity in the auditory pathway of barn owls (Gerstner, Kempter, van Hemmen, & Wagner, 1996). Recent work investigates the stabilization capabilities of asymmetric rules in keeping the cell's sensitivity (Kempter et al., 1999b; Abbott & Song, 1999), similarly as it is achieved by the described sliding-threshold property on the level of mean firing rates. Neither of these works, however, take into account the synaptic dynamics.

Our algorithm comes closest to the version of the learning rule outlined in Gerstner, Kempter, van Hemmen, and Wagner (1998, sec. 14.2.4), which deals with the kinetics of four different components corresponding to our N_u, N_d, S_u, and S_d. In their description, no synaptic depression is taken into account, and the rule refers to a change in the absolute synaptic strength. Moreover, no common pool similar to N_{rec} is assumed, and Hebbian second-order correlations are only considered. It is worth pointing out that the physiologically motivated restriction to a common pool N_{rec} may help to sharpen the distinction between positive and negative spike delays, even in the case of a deterministic release without depression. Considering simultaneous bursts of pre- and postsynaptic spikes of mixed temporal correlations, it would typically be the first release-spike pair that, due to the depletion of the common pool, dominates the synaptic modification. An immediately following second pair with possible reversed temporal order will be much less effective if this pool was just reduced and therefore will not be able to annihilate the initiated modification.

In comparison to rules based on mean firing rates one may establish connections to the BCM theory (Bienenstock et al., 1982) but also reproduce the rule of Artola-Bröcker-Singer (Artola & Singer, 1993) by assuming nonvanishing thresholds for the up- and downregulation. On the other hand, the simplified form, equation 3.5, shows that our algorithm is distinct from the covariance rule (Sejnowski, 1977), which in our situation would be of the

form

$$\triangle P_{dis} \approx (f_{pre}^{rel} - \langle f_{pre}^{rel} \rangle)\,(f_{post}^{sp} - \langle f_{post}^{sp} \rangle),$$

and therefore would be symmetric with respect to the presynaptic release and the postsynaptic spike frequencies. The power of our algorithm is not only to cope with average firing frequencies and correlations but to offer a general framework for dealing with any pre- and postsynaptic spike train of any complexity and arbitrary correlations.

4.4 Predictions of the Model and Outlook. It is remarkable that simple first-order kinetics with a cross-gating of the NMDA receptors can qualitatively explain the different spike-induced nonlinear synaptic modifications. Several features of the model are tailored to explain the specific experimental results and raise new hypotheses that can be experimentally tested. Among these are the following:

1. Experiment 2 with a reversed relative timing would lead to a moderate monotonic decrease of P_{dis} with respect to the paired spike frequency (contrasting Figure 4).
2. Experiment 2 with 20 instead of 5 spikes in the paired spike trains would lead to a nonmonotonic P_{dis} with respect to frequency (see Figure 5).
3. The full learning curve for trains of 5 spikes versus the time difference of the train onsets would exhibit a maximal upregulation and maximal downregulation at -50 ms and 100 ms, respectively (see Figure 6b).
4. Applying pre- and postsynaptic Poisson spike trains would lead to a monotonic increase of the steady-state P_{dis} with respect to the postsynaptic frequency and to only a small decrease with respect to the presynaptic frequency (see Figure 7b).
5. A step change in the frequency of the postsynaptic Poisson spike train after a period of steady-state Poisson stimulations would lead to a decrease or increase in P_{itdis} depending on the sign of the step change (see Figure 8b).
6. Modulating sinusoidally the frequencies of pre- and postsynaptic Poisson spike trains of lag 0 would lead to an increase in P_{dis} if the modulation frequency is in the range of 1 Hz but would not show any change if the modulation rate is faster than 5 Hz (see Figure 7).
7. A single presynaptic release followed by a burst of postsynaptic spikes would lead to a superlinear increase of P_{dis} with respect to the burst frequency before eventually saturating.

The last experiment appears to be of particular interest in the light of recently observed Ca^{2+}-triggered bursts in cortical pyramidal cells following coincident apical and somatic stimulations (Larkum, Zhu, & Sakmann,

1999). The threshold phenomenon according to which virtually no potentiation is seen for a 1 Hz pairing suggests that these bursts are functionally relevant in the existing form of synaptic modifications. It also suggests that an incidentally occurring tight pairing would not be able to change the synaptic memory. Finally, more natural stimulation protocols, including bursts and Poisson trains, would help to specify the activity dependencies of the learning window, which is partially expressed in the data. It would also clarify the question to what extent the same synapse is able to encode individual spike timings while still being sensitive to pre- and postsynaptic average frequencies.

To describe further long-term potentiation and long-term depression experiments, one may want to include effects of the postsynaptic membrane potential or the local Ca^{2+} concentration onto the NMDA receptor dynamics or the secondary messenger activation. Although we have not examined this, it could easily be achieved by endowing the different rate constants appearing in the scheme with a voltage- or Ca^{2+}-dependent dynamics instead of instantaneously activating them through delta functions of fixed weights.

Beside the characteristics of strong synaptic depression, a large heterogeneity of different synaptic dynamics including facilitation was found between neocortical pyramidal cells (Markram, Pikus, Gupta, & Tsodyks, 1998), suggesting that other parameters governing the temporal response could be subject to specific learning rules (Markram, Wang, & Tsodyks, 1998). One could speculate that due to additional computation such as the integration of a third coincident signal provided by growth factors or neuromodulators (e.g., synaptic growth or unmasking of postsynaptic receptors; Liao & Malinow, 1995) is required for the induction of real synaptic strengthening or to gate changes in the recovery time constant. Specifying these conditions remains an important challenge for a future research.

Appendix

A.1 Differential Equations Determining the Kinetic Scheme. For further analysis we give a formulation of the kinetic scheme (see Figure 2) in terms of differential equations. Let us denote by t_{pre}^{rel} the time of a presynaptic release and by t_{post}^{sp} the time of a postsynaptic spike. A presynaptic release at t_{pre}^{rel} will saturate a fraction r_u^N of the recovered NMDA receptors. A postsynaptic spike at t_{post}^{sp} will block the fraction r_d^N of N_{rec}. The entire dynamics of the NMDA receptors is:

$$\frac{dN_u}{dt} = -\frac{N_u}{\tau_u^N} + r_u^N N_{rec}\,\delta(t - t_{pre}^{rel}), \tag{A.1}$$

$$\frac{dN_d}{dt} = -\frac{N_d}{\tau_d^N} + r_d^N N_{rec}\,\delta(t - t_{post}^{sp}), \tag{A.2}$$
$$N_{rec} = 1 - N_d - N_u,$$

where the delta function $\delta(\ldots)$ expresses that the quantities N_u and N_d have to be augmented at the times of a presynaptic release and a postsynaptic spike by $r_u^N N_{rec}$ and $r_d^N N_{rec}$, respectively.

The differential equations for the secondary messengers are:

$$\frac{dS_u}{dt} = -\frac{S_u}{\tau_u^S} + r^S N_u(1 - S_u)\,\delta(t - t_{post}^{sp}), \tag{A.3}$$
$$\frac{dS_d}{dt} = -\frac{S_d}{\tau_d^S} + r^S N_d(1 - S_d)\,\delta(t - t_{pre}^{rel}). \tag{A.4}$$

The time constants τ_u^S and τ_d^S encompass a diffusion process and are in the range of 300 ms. The limit probability is upregulated at a postsynaptic spike if S_u exceeds some threshold S_u^θ and downregulated at a presynaptic release if S_d exceeds some threshold S_d^θ. According to the kinetic scheme, we have

$$\begin{aligned}\frac{dP_{dis}^\infty}{dt} &= r_u^P(1 - P_{dis}^\infty)[S_u^+ - S_u^\theta]^+\,\delta(t - t_{post}^{sp}) \\ &\quad - r_d^P P_{dis}^\infty[S_d^+ - S_d^\theta]^+\,\delta(t - t_{pre}^{rel}),\end{aligned} \tag{A.5}$$

where S_u^+ and S_d^+ are the values of S_u and S_d immediately after a post- and presynaptic spike,

$$S_u^+ = r^S N_u\,(1 - S_u) + S_u, \quad S_d^+ = r^S N_d\,(1 - S_d) + S_d. \tag{A.6}$$

Taking the expectation values in equation A.5 leads to equation 3.1. While the changes in P_{dis}^∞ occur instantaneously, the discharge probability P_{dis} slowly approaches the limit probability according to the equation

$$\frac{dP_{dis}}{dt} = \frac{P_{dis}^\infty - P_{dis}}{\tau_M^P}, \qquad \text{with} \quad \tau_M^P \approx 10\,\text{min}. \tag{A.7}$$

A.2 Equations Determining the Probability of Release. A synapse is assumed to have a single site of release from which, according to the univesicular hypothesis, a single vesicle discharges with probability P_{dis} at the arrival of a presynaptic spike. Instantaneously after discharge, the site of release is empty, and it is assumed to be reoccupied by a new vesicle in a Poisson process with time constant $\tau_v^{rec} \approx 800$ ms. The probability P_v that

a vesicle is at the site of release is therefore governed by the differential equation,

$$\frac{dP_v}{dt} = \frac{1 - P_v}{\tau_v^{rec}} - P_{dis} P_v \, \delta(t - t_{pre}^{sp}), \tag{A.8}$$

where t_{pre}^{sp} is the time a presynaptic spike arrives. This equation states that at the time of a presynaptic spike, P_v is reset with probability P_{dis} from its actual state back to 0. The probability P_v^{n+1} of encountering a vesicle ready for release at arrival of the $(n+1)$th spike is now calculated by

$$P_v^{n+1} = P_v^n (1 - P_{dis}) \, e^{-\frac{\triangle_n}{\tau}} + (1 - e^{-\frac{\triangle_n}{\tau}}), \qquad \tau = \tau_v^{rec},$$

where $\triangle_n = t_{pre}^{sp,n+1} - t_{pre}^{sp,n}$ is the time elapsed between the two spikes and P_v^n is the probability that a vesicle was ready at the previous spike. Since the probability of release for a presynaptic spike is $P_{rel} = P_{dis} P_v$, we get formula 2.1. The instantaneous release frequency is calculated from the presynaptic spike frequency according to

$$f_{pre}^{rel} = P_{rel} \, f_{pre}^{sp} = P_{dis} \, P_v \, f_{pre}^{sp} \, . \tag{A.9}$$

For presynaptic Poisson spike trains of rate f_{pre}^{sp}, one can calculate from equation A.8 the steady-state release probability by

$$P_{rel}^{ss} = P_{dis} P_v^{ss} = \frac{P_{dis}}{1 + P_{dis} \, f_{pre}^{sp} \, \tau_v^{rec}} \, .$$

The release frequency at steady state is then given by $f_{pre}^{rel} = P_{rel}^{ss} f_{pre}^{sp}$. Note that due to the memory in the recovery process, the release train is not Poissonnian anymore.

A.3 Steady-State Equations for Poisson Spike Trains. We deduce the steady state of the limit probability of vesicle discharge, $P_{dis}^{\infty ss}$, for pre- and postsynaptic Poisson spike trains with fixed rates f_{pre}^{sp} and f_{post}^{sp}. Since the time constant τ_M^P for modification is large, we may assume that P_{dis} remains constant even during the steady-state stimulation. In the following, we calculate the steady-state value of P_{dis}^{∞} toward which P_{dis} converges after the stimulation according to equation 4.7.

First, we consider the steady states of the NMDA receptors and the secondary messengers. Replacing the delta functions in equations A.1 through A.4 with the corresponding rates f_{pre}^{rel} and f_{post}^{sp}, we obtain the following expectation value in the steady state:

$$N_u^{ss} = \frac{\rho_u^N \, f_{pre}^{rel}}{1 + \rho_u^N \, f_{pre}^{rel} + \rho_d^N \, f_{post}^{sp}}, \qquad \rho_u^N = r_u^N \tau_u^N, \tag{A.10}$$

$$N_d^{ss} = \frac{\rho_d^N f_{post}^{sp}}{1 + \rho_u^N f_{pre}^{rel} + \rho_d^N f_{post}^{sp}}, \qquad \rho_d^N = r_d^N \tau_d^N, \tag{A.11}$$

$$S_u^{ss} = \frac{\rho_u^S f_{post}^{sp} N_u^{ss}}{1 + \rho_u^S f_{post}^{sp} N_u^{ss}}, \qquad \rho_u^S = r^S \tau_u^S, \tag{A.12}$$

$$S_d^{ss} = \frac{\rho_d^S f_{pre}^{rel} N_d^{ss}}{1 + \rho_d^S f_{pre}^{rel} N_d^{ss}}, \qquad \rho_d^S = r^S \tau_d^S. \tag{A.13}$$

Note that due to the shared pool N_{rec}, the variables N_x and S_x ($x = u, d$) are not independent, and that, strictly speaking, we are not allowed to average the product in equations A.3 and A.4 individually. However, as long as one of the frequencies f_{post}^{sp} and f_{pre}^{rel} is small compared to the time constants τ_x^N and τ_x^S, one of the variables N_x and S_x always has time to relax toward its mean between the jumps of the other. Indeed, for $\tau_v^{rec} \approx 1$, the release rate will be less than ≈ 1 Hz, while the time constants in consideration are all smaller than ≈ 0.5 second and formulas A.12 and A.13 turn out to be a good approximation (cf. Figure 7a). Also, the error we are handling by treating f_{pre}^{rel} as a Poisson rate seems to be marginal. By a similar reasoning we may average the individual factors in equation A.5 to obtain

$$0 = r_u^P (1 - P_{dis}^{\infty\,ss}) \, [S_u^+ - S_u^\theta]^{+\,ss} \, f_{post}^{sp} - r_d^P P_{dis}^{\infty\,ss} \, [S_u^+ - S_u^\theta]^{+\,ss} \, f_{pre}^{rel}, \tag{A.14}$$

where the superscript ^{ss} denotes the expectation value of the corresponding quantity in the steady state. If the variation of S_x is small, the quantity $[S_x^+ - S_x^\theta]^{+\,ss}$ can be approximated by $[S_x^{+\,ss} - S_x^\theta]^+$, and in case of vanishing thresholds $S_x^\theta = 0$, it is equal to

$$S_x^{+\,ss} = r^S N_x^{ss} (1 - S_x^{ss}) + S_x^{ss}, \qquad x \in \{u, d\}. \tag{A.15}$$

In this case one obtains from equation A.14 the expectation value of P_{dis}^∞ in the steady state,

$$P_{dis}^{\infty\,ss} = \frac{1}{1 + \frac{r_d^P f_{pre}^{rel} S_d^{+\,ss}}{r_u^P f_{post}^{sp} S_u^{+\,ss}}}, \tag{A.16}$$

which in general is a good approximation if S_x^+ is above the threshold S_x^θ most of the time.

It is elusive to study the transition from the full model to the reduced model, which considers only the cross-gating of the NMDA receptors without secondary messengers. From equation A.5 we get at steady state with

vanishing thresholds

$$\frac{dP_{dis}^{\infty}}{dt} = r_u^P(1 - P_{dis}^{\infty^{ss}})S_u^{+^{ss}}\, f_{pos}^{sp} - r_d^P P_{dis}^{\infty^{ss}} S_d^{+^{ss}}\, f_{pre}^{rel}. \tag{A.17}$$

Linearizing N_x^{ss} and S_x^{ss} (see equations A.10–A.13) around zero frequencies (thereby neglecting saturation effects) and inserting into equation A.15 yields

$$S_u^{+^{ss}} \approx \tilde{\rho}_u^N\, f_{pre}^{rel}(1 - \tilde{\rho}_u^S \tau_u^S\, f_{pos}^{sp}\, f_{pre}^{rel}) + \tilde{\rho}_u^S \tau_u^S\, f_{pos}^{sp}\, f_{pre}^{rel} \tag{A.18}$$

$$S_d^{+^{ss}} \approx \tilde{\rho}_d^N\, f_{pre}^{rel}(1 - \tilde{\rho}_d^S \tau_d^S\, f_{pre}^{rel}\, f_{post}^{sp}) + \tilde{\rho}_d^S \tau_d^S\, f_{pre}^{rel}\, f_{post}^{sp}, \tag{A.19}$$

with appropriate constants $\tilde{\rho}_x^X$. If $\tau_u^S\, f_{pos}^{sp}$ and $\tau_d^S\, f_{pre}^{rel}$ are small, the second and third terms in equations A.18 and A.19 vanishes, and the synaptic change is dominated by the second-order correlations,

$$\frac{dP_{dis}^{\infty}}{dt} \approx \tilde{r}_u^P(1 - P_{dis}^{\infty^{ss}}) f_{pre}^{rel}\, f_{pos}^{sp} - \tilde{r}_d^P P_{dis}^{\infty^{ss}}\, f_{post}^{sp}\, f_{pre}^{rel}.$$

This is true if in particular $\tau^S = 0$ (and the secondary messengers therefore act only by a constant factor). If, on the other hand, $\tau_u^S\, f_{pos}^{sp}$ and $\tau_d^S\, f_{pre}^{rel}$ are large, the secondary messengers are closer to saturation ($S_x^{ss} \approx 1$), the second term in equations A.18 and A.19 is now dominating, and a third-order correlation enters in equation A.17. This reasoning also motivates the short forms (see equations 3.5 and 3.6) of the learning rule for the nonsteady-state situation and the cases $\tau^S = 0$ and $\tau^S > 1/f$, respectively.

A.4 Deduction of the BCM Properties. To show the connection to the BCM theory (Bienenstock et al., 1982) we assume $S_d^{\theta} = 0$ and consider our learning rule, equation 3.1. Inserting the parameters into equation A.5 shows that the time constant of P_{dis}^{∞} is of an order slower than that of S_u and S_d (see Figures 7a and 8a). In the limit of slow adapation of P_{dis}^{∞}, we may thus replace the quantities S_u^+ and S_d^+ by their steady-state values. Writing the learning rule in the form 3.2, we obtain

$$\phi(f_{post}^{sp}) = (1 - P_{dis}^{\infty})\,[S_u^{+^{ss}} - S_u^{\theta}]^+ \frac{f_{post}^{sp}}{f_{pre}^{rel}} - \frac{r_d^P}{r_u^P} P_{dis}^{\infty}\, S_d^{+^{ss}}. \tag{A.20}$$

We have to show that this function satisfies the requirements of the BCM learning curves. The first requirement $\phi(0) = 0$ is readily checked since $S_d^{+^{ss}}$ vanishes for $f_{post}^{sp} = 0$ according to equations A.11 and A.13. We have $\phi'(0) < 0$ since for small f_{post}^{sp}, the second term in equation A.20 will dominate for $r_d^P > 0$. This is true since the first term is bound from above by $(f_{post}^{sp})^2$,

and the second term is bound from below by f^{sp}_{post}. Since for large f^{sp}_{post}, it is the first term in equation A.20, which dominates, we get a second zero of ϕ at

$$\theta_M = \frac{r^P_d}{r^P_u} \frac{P^\infty_{dis}}{(1 - P^\infty_{dis})} \frac{S^{+ss}_d}{[S^{+ss}_u - S^\theta_u]^+} f^{rel}_{pre} \tag{A.21}$$

with $\phi'(\theta_M) \geq 0$. The modification threshold is implicitly driven by the postsynaptic spike rate f^{sp}_{post}, which changes S^{+ss}_u and S^{+ss}_d via equations A.10 through A.13, and this in turn changes P^∞_{dis} via learning rule 3.2. The convergence of P^∞_{dis} for fixed frequencies ensures that eventually the right-hand side of equation 3.2 vanishes, and this, by definition, happens when $\theta_M = f^{sp}_{post}$. For example, if f^{sp}_{post} grows over θ_M, we have $\phi(f^{sp}_{post}) > 0$ and the learning rule pushes P^∞_{dis} up. Due to the factor $P^\infty_{dis}/(1 - P^\infty_{dis})$, however, the threshold θ_M increases as well. Since the speed of θ_M is nonlinear in P^∞_{dis}, this factor dominates the (saturating) changes in S^{+ss}_u and S^{+ss}_d. The threshold θ_M will therefore eventually catch up and overtake f^{sp}_{post}, and we get $\phi(f^{sp}_{post}) < 0$. According to the learning rule, P^∞_{dis} now starts to decrease again. Hence, equation A.21 incorporates the sliding threshold property with respect to f^{sp}_{post}, and this keeps the synapse sensitive to its environment.

A.5 Change of P^∞_{dis} for Nonzero Spike Correlations. We first quantify the effect of the spike correlation onto the distribution of the up- and down-regulating quantities N_u and N_d in their steady states. Recall that for a spike correlation of, say, $c_s = 1$, each postsynaptic spike follows instantaneously after a presynaptic spike. For a positive spike correlation $c_s \in [0, 1]$, the effective postsynaptic frequency is reduced by the fraction $r^N_u [c_s]^+ P^{ss}_{rel}$, and we must replace f^{sp}_{post} by $(1 - r^N_u [c_s]^+ P^{ss}_{rel})\, f^{sp}_{post}$ in the formulas A.10 and A.11, giving the average values of N_u and N_d, respectively. Similarly, for a negative spike correlation $c_s \in [-1, 0]$, the presynaptic release frequency f^{rel}_{pre} must be replaced by $(1 - r^N_d [-c_s]^+)\, f^{rel}_{pre}$ in the same two formulas, and the steady states N^{ss}_u and N^{ss}_u become functions of c_s. Next, in formulas A.12, A.13, and A.15, the quantities N^{ss}_u and N^{ss}_u have to be replaced by their average values immediately after a pre- or postsynaptic spike, that is, by $N^{ss^+}_u = N^{ss}_u + r^N_u [c_s]^+ P^{ss}_{rel} N^{ss}_{rec}$ and $N^{ss^+}_d = N^{ss}_d + r^N_d [-c_s]^+ N^{ss}_{rec}$, respectively. (Since due to the memory in the vesicle recovery process the presynaptic release train is not Poissonian, we would not be allowed to replace the delta function by the release rate to calculate the mean-field behavior. If in addition there is a nonvanishing correlation between the pre- and postsynaptic spike trains, this "simplification" indeed cannot be neglected anymore. We were urged to correct the mean-field plots in Figure 10 empirically by a factor of 1.3 in front of c_s.) If we now put $S^\theta_u = S^\theta_d = 0$ we get from equation A.14 the steady state of P^∞_{dis} as a function of the spike correlation c_s (see

Figure 10b). The mean-field evolution of P_{dis}^{∞} for a given spike correlation $c_s \in [-1, 1]$ is obtained by the analog replacements (while dropping the upper index ^{ss}) in formulas A.1 through A.4 and A.6.

Acknowledgments

This study was supported by the Priority Program Biotechnology of the Swiss National Foundation (grant 21-57076.99) (W. S.), the Office of Naval Research, the Human Frontier Science Program Organization, and the Israeli Academy of Sciences (H. M. and M. T.).

References

Abbott, L. (1996). Decoding neuronal firing and modeling neural networks. *Quart. Rev. Biophys., 27*, 291–331.

Abbott, L., & Song, S. (1999). Temporally asymmetric Hebbian learning, spike timing and neuronal response variability. In M. Kearns, S. Solla, & D. Cohn (Eds.), *Advances in neural information processing systems, 11*. Cambridge, MA: MIT Press.

Abbott, L., Varela, J., Sen, K., & Nelson, S. (1997). Synaptic depression and cortical gain control. *Science, 275*, 220–224.

Antonov, S., Gmiro, V., & Johnson, J. (1998). Binding sites for permeant ions in the channel of NMDA receptors and their effects on channel block. *Nature Neuroscience, 1*(6), 451–461.

Artola, A., & Singer, W. (1993). Long-term depression of excitatory synaptic transmission and its relationship to long-term potentiation. *Trends in Neurosci., 16*(11), 480–487.

Bear, M., Cooper, L. N., & Ebner, F. F. (1987). A physiological basis for a theory of synapse modification. *Science, 237*, 42–48.

Bell, C., Han, V., Sugawara, Y., & Grant, K. (1997). Synaptic plasticity in a cerebellum-like structure depends on temporal order. *Nature, 387*(6630), 278–281.

Bi, G., & Poo, M. (1998). Precise spike timing determines the direction and extent of synaptic modifications in cultured hippocampal neurons. *J. Neurosci., 18*, 10464–10472.

Bienenstock, E., Cooper, L., & Munro, P. (1982). Theory for the development of neuron selectivity: Orientation specificity and binocular interaction in visual cortex. *J. Neurosci., 2*(1), 32–48.

Blum, K., & Abbott, L. (1996). A model of spatial map formation in the hippocampus of the rat. *Neural Computation, 8*(1), 85–93.

Brown, T. H., & Chatterji, S. (1994). Hebbian synaptic plasticity: Evolution of the contemporary concept. In E. Domany, J. van Hemmen, & K. Schulten (Eds.), *Model of neural networks II* (pp. 287–314). Berlin: Springer.

Debanne, D., Shulz, D., & Fregnac, Y. (1995). Temporal constraints in associative synaptic plasticity in hippocampus and neocortex. *Can. J. Physiol. and Pharmacol., 73*, 1295–1311.

Fregnac, Y., & Shulz, D. (1994). Models of synaptic plasticity and cellular analogs of learning in the developing and adult visual cortex. In V. Casagrande & P. Shinkman (Eds.), *Advances in neural and behavioral development* (4th ed.). Norwood, NJ: Ablex.

Fregnac, Y., Shulz, D., Thorpe, S., & Bienenstock, E. (1988). A cellular analogue of visual cortical plasticity. *Nature, 333*, 367–370.

Fusi, S., Annunziato, M., Badoni, D., Salamon, A., & Amit, D. J. (2000). Spike-driven synaptic plasticity: Theory, simulation, VLSI implementation. *Neural Computation, 12*(10), 2257–2258.

Gerstner, W., & Abbott, L. (1997). Learning navigational maps through potentiation and modulation of hippocampal place cells. *J. Comput. Neuroscience, 4*, 79–94.

Gerstner, W., Kempter, R., van Hemmen, J., & Wagner, H. (1996). A neuronal learning rule for sub-millisecond temporal coding. *Nature, 383*, 76–78.

Gerstner, W., Kempter, R., van Hemmen, J., & Wagner, H. (1998). Hebbian learning of pulse timing in the barn owl auditory system. In W. Maass & C. Bishop (Eds.), *Pulsed neural networks*. Cambridge, MA: MIT Press.

Grzywaca, N., & Burgi, P.-Y. (1998). Toward a biophysically plausible bidirectional Hebbian rule. *Neural Compuation, 10*, 499–520.

Gustafsson, B., Wigström, H., Abraham, W., & Huang, Y.-Y. (1987). Long-term potentiation in the hippocampus using depolarizing current pulses as the conditioning stimulus to single volley synaptic potentials. *J. Neurosci., 7*, 774–780.

Hebb, D. O. (1949). *The organization of behaviour*. New York: Wiley.

Hopfield, J. (1995). Pattern recognition computation using action potential timing for stimulus representation. *Nature, 376*, 33–36.

Jonas, P., & Spruston, N. (1994). Mechanisms shaping glutamate-mediated excitatory postsynaptic currents in the CNS. *Curr. Opin. Neurobiol., 4*(3), 366–372.

Kempter, R., Gerstner, W., & van Hemmen, J. (1999a). Hebbian learning and spiking neurons. *Physical Review E, 59*(4), 4498–4514.

Kempter, R., Gerstner, W., & van Hemmen, J. (1999b). Spike-based compared to rate-based Hebbian learning. In M. S. Kearns, S. Solla, & D. Cohn (Eds.), *Advances in neural information processing systems, 11*. Cambridge, MA: MIT Press.

Larkum, M., Zhu, J., & Sakmann, B. (1999). A novel cellular mechanism for coupling inputs arriving at different cortical layers. *Nature, 398*, 338–341.

Liao, D., & Malinow, N. H. R. (1995). Activation of postsynaptically silent synapses during pairing-induced LTP in CA1 region of hippocampal slice. *Nature, 375*, 400–404.

Maass, W. (1998). A simple model for neural computation with firing rates and firing correlations. *Network: Computation in Neural Systems, 9*(3), 381–397.

Markram, H., Helm, P., & Sakmann, B. (1995). Dendritic calcium transients evoked by single back-propagating action potentials in rat neocortical pyramidal neurons. *J. Physiol. (London), 485*, 1–20.

Markram, H., Lübke, J., Frotscher, M., & Sakmann, B. (1997). Regulation of synaptic efficacy by concidence of postsynaptic APs and EPSPs. *Science, 275*, 213–215.

Markram, H., Pikus, D., Gupta, A., & Tsodyks, M. (1998). Potential for multiple mechanisms, phenomena and algorithms for synaptic plasticity at single synapses. *Neuropharmacology, 37*, 489–500.

Markram, H., Roth, A., & Helmchen, F. (1998). Competitive calcium binding: Implications for dendritic calcium signaling. *JCNS, 5*(3), 331–348.

Markram, H., & Tsodyks, M. (1996). Redistribution of synaptic efficacy between neocortical pyramidal neurons. *Nature, 382*, 807–810.

Markram, H., Wang, Y., & Tsodyks, M. (1998). Differential synaptic transmission via the same axon from neocortical layer 5 pyramidal neurons. *PNAS, 95*, 5323–5328.

Mayer, M. (1998). Ion-binding sites in NMDA receptors: Classical approaches provide the numbers. *Nature Neuroscience, 1*(6), 433–434.

Mayer, M., McDermott, A., Westbrook, G., Smith, S., & Barker, J. (1987). Agonist- and voltage-gated calcium entry in cultured mouse spinal cord neurons under voltage clamp measured using Arsenazo III. *J. Neurosci., 7*, 3230–3244.

Medina, I., Filippova, N., Bakhramov, A., & Bregestovski, P. (1996). Calcium-induced inactivation of NMDA receptor-channels evolves independently of run-down in cultured rat brain neurones. *J. Physiol. (London), 495*, 411–427.

Oja, E. (1982). A simplified neuron model as a principal component analyzer. *J. Math. Biol., 15*, 267–273.

Sejnowski, T. (1977). Storing covariance with nonlinearly interacting neurons. *J. Math. Biol., 4*, 303–321.

Senn, W., Tsodyks, M., & Markram, H. (1997). An algorithm for synaptic modification based on exact timing of pre- and post-synaptic action potentials. In W. Gerstner, A. Germond, M. Hasler, & J.-D. Nicoud (Eds.), *Artificial Neural Networks—ICANN'97* (pp. 121–126). Berlin: Springer-Verlag.

Spruston, N., Jonas, P., & Sakmann, B. (1995). Dendritic glutamate receptor channels in rat hippocampal CA3 and CA1 pyramidal neurons. *J. Physiol. (London), 482*, 325–352.

Stanton, P., & Sejnowski, T. (1989). Associative long-term depression in the hippocampus induced by Hebbian covariance. *Nature, 339*, 215–218.

Triller, A., & Korn, H. (1982). Transmission at a central inhibitory synapse. III: Ultrastructure of physiologically identified and stained terminals. *J. Neurophysiol., 48*, 708–736.

Tsodyks, M., & Markram, H. (1997). The neural code between neocortical pyramidal neurons depends on neurotransmitter release probability. *Proc. Natl. Acad. Sci. USA, 94*, 719–723.

Tsumoto, T. (1990). Long-term potentiation and depression in the cerebral neocortex. *Jpn. J. Physiol., 40*, 573–593.

Zhang, L., Tao, H., Holt, C., Harris, W., & Poo, M. (1998). A critical window in the cooperation and competition among developing retinotectal synapses. *Nature, 395*, 37–44.

Received October 14, 1998; accepted March 21, 2000.